MODELING KARST AQUIFER RESPONSE TO RAINFALL

by

Winfield G. Wright

Thesis submitted to the Graduate Faculty of the
Virginia Polytechnic Institute and State University
in partial fulfillment of the requirements of the degree of
MASTER OF SCIENCE
in
Civil Engineering

APPROVED:

J. M. Wiggert, Chairman

T. Kuppusamy, Co-chairman

J. H. Sherrard

February, 1986

Blacksburg, Virginia

MODELING KARST AQUIFER RESPONSE TO RAINFALL

by

Winfield G. Wright

(ABSTRACT)

A finite-element model (HYDMATCH) uses spring hydrograph discharge data to generate a linear regression relation between fracture conductivity and potential gradient in a karst aquifer system. Rainfall excess in the form of potential energy from sinkhole sub-basins is input to element nodes and routed through a one-dimensional finite-element mesh to the karst spring represented by the last node in the finite element mesh. A fracture-flow equation derived from the Navier-Stokes equation uses fracture conductivities from the regression equation and potential gradient in the last element of the mesh to determine discharge at the spring.

Discharge hydrograph data from Nininger spring, located in Roanoke, Virginia, was used to test the performance of the model. Excess from a one-half inch rain was introduced into sinkhole nodes and the regression equation generated by matching discharges from the known hydrograph for the one-half inch rainfall. New rainfall excess data from a one-inch rainfall was input to the sinkhole nodes and routed through the finite-element mesh. The spring hydrograph for the one-inch rainfall was calculated using the regression equation which was

determined previously. Comparison of the generated hydrograph for the one-inch rainfall to a known hydrograph for a one-inch rainfall shows similar shapes and discharge values.

Areas in need of improvement in order to accurately model ground-water flow in karst aquifers are a reliable estimate of rainfall excess, a better estimation of baseflow and antecedent aquifer conditions, and the knowledge of the karst aquifer catchment boundaries. Models of this type may then be useful to predict flood discharges and contaminant travel times in karst aquifers.

TABLE OF CONTENTS

LIST OF ILLUSTRATIONS

LIST OF TABLES

CHAPTER 1

INTRODUCTION

Karst is defined as the irregular landforms that develop on limestone and dolomite terranes by the solution of surface and ground waters forming characteristic features such as sinkholes, non-integrated surface valleys, and subsurface conduits which transmit ground water. The absence of surface streams and the presence of resurging springs are characteristics of karst areas. Karst ground-water aquifers frequently cause construction and pollution problems in limestone areas of population development due to the unknown occurence of cavities and rapid ground-water flow paths.

Limestone aquifers differ from aquifers composed of other material types due to the solutional enlarging of fissures or fractures. If the path of ground-water flow is through an area-wide network of interconnected fissures, then conventional methods of aquifer evaluation may be applied with the exception of anisotropic permeabilities. The problems with theoretical analysis arise when limestone aquifers consist of discrete, well-developed conduits. Considerable effort has gone into attempts to understand conduit systems. Many efforts describing hydrogeologic controls on karst aquifers are reviewed by Stringfield and LeGrand (1969) and LeGrand (1973).

Analysis of the spring hydrograph is a tool available for karst aquifer evaluation. The hydraulic parameters (permeability and storage) of karst aquifers have been determined by applying the Theis equation to the recession curves of spring hydrographs (Tobarov, 1976). Problems arise using this method due to different linear segments of the log-log recession curve. White (1969) used the base-flow recession curve to determine drainage basin coefficients (discharge ratio, exhaustion coefficient, and response time).

Digital modeling has potential for the evaluation of karst aquifer parameter analysis. Thrailkill (1974) adopted equivalent pipe-flow systems to predict flow directions and head distribution within a karst system using the finite-difference method. Few other efforts have shown any success in simulating the flow of water through spring discharging karst systems in response to recharge due to rainfall.

The objective of this study is to model rainfall-runoff and spring discharges in karst areas. Overland flow are modeled using equations approximating rainfall-runoff on a sloped surface. The characteristics of karst spring hydrographs are used to estimate the hydraulic parameters of a karst aquifer. Introduction of excess rainfall and propagation of storm pulses through the fractured-aquifer system are modeled using the finite-element method. The finite-element model constructed determines representative fracture conductivities-- using

an equation for fluid flow through a fracture -- of a karst aquifer by iterating fracture conductivity in the system until the hydrograph from a known rainfall event is matched. A linear regression is established for potential gradients in the karst aquifer system versus fracture conductivities. The model is verified by comparing known spring hydrograph discharges from another rainfall event to modeled discharges for that rainfall event.

CHAPTER 2

HYDRAULICS OF KARST AQUIFERS

Karst aquifers which cause the most theoretical difficulties in parameter evaluation are the aquifers which are dominated by fissures and conduits. The problem originates with the hydrogeological setting of conduit development. Moving ground water may select bedding plane partings or may follow fractures and faults in the limestone. The result of calcite dissolution along these paths of water movement is tubular or fissure-like conduits. The ground water will move down-gradient along these openings much easier than it will move through the primary pores of the limestone. Secondary permeablities are developed due to these openings. Ground water flowing through this type of system may not flow at right angles to potentiometric contours and may not coincide with the contour of the land surface.

Rainfall-runoff Relationships

To understand the way a karst basin functions, try to imagine a number of large funnels covered with soils of varying depths and differing vegetation. When rain falls on these funnels, the resulting input to the karst aquifer from a sinkhole funnel would be an overland flow hydrograph due to rainfall excess. The shape of the sub-basin

hydrograph depends on the antecedent soil-moisture condition and the roughness of the vegetation and ground surface with respect to flowing water. Flow from the center of the funnel travels down a conduit to an intersection with a conduit carrying flow from another funnel. Together, the combined flows travel to the spring outlet of the aquifer increasing in flow quantity with the addition of each funnel's runoff. The funnels have different areas so the peaks from each funnel will be of different timing and magnitude. Overland flow recession at the funnel inputs will be different depending on sinkhole sub-basin characteristics.

Overland Flow

The overland flow aspect of rainfall-runoff was modeled using Izzard's time-lag approximation for surface runoff (Chow, 1959, p. 542). Izzard's equations use roughness factor, slope, length and width of runoff plane. Equilibrium discharge is calculated for a particular rainfall by:

$$QE(N) = (R - F) \times RL / 43{,}200 \qquad (1)$$

where: QE(N) = equilibrium discharge in subbasin N, per unit foot of runoff plane width,
R = rainfall, inches per hour,
RL = length of runoff plane, feet,
and, F = infiltration rate, inches per hour.

Infiltration can be calculated using an equation developed by Holtan and Lopez(1971) as follows:

$$F = GI \times A \times SS \times C + FC \qquad (2)$$

where: GI = seasonal index for infiltration,
A = Holtan's coefficient for cover conditions,
SS = depth of the 'A' horizon,
C = ratio of potential gravitational water to potential plant available water in the soil,
and, FC = infiltration capacity, inches per hour.

The coefficients F, SS, and FC were obtained from U.S. Soil Conservation (SCS) data. The values for GI, A, and C were obtained from Holtan's publication.

To determine overland-flow discharges, equilibrium time is calculated as follows:

$$TE(N) = 2 \times DE(N) \;/\; 60 \times QE(N) \qquad (3)$$

where: $DE(N) = RK \times RL \times QT$
$RK = 0.0007 \times R + RC \;/\; S^{1/3}$,
$QT = 1 \;/\; QF^{1/3}$,
$QF = 1 \;/\; QE(N)$,
RC = roughness of runoff plane,
and, S = slope of runoff plane.

The values for runoff plane length, slope, and width are obtained from topographical maps.

For particular time increments, the time values from the beginning of the storm event until the storm duration are divided by TE(N) for each subbasin N . Using the dimensionless hydrograph(figure 1), dimensionless discharges for overland flow are determined by selecting dimensionless values of q/q_e corresponding to each t/t_e. Discharge is

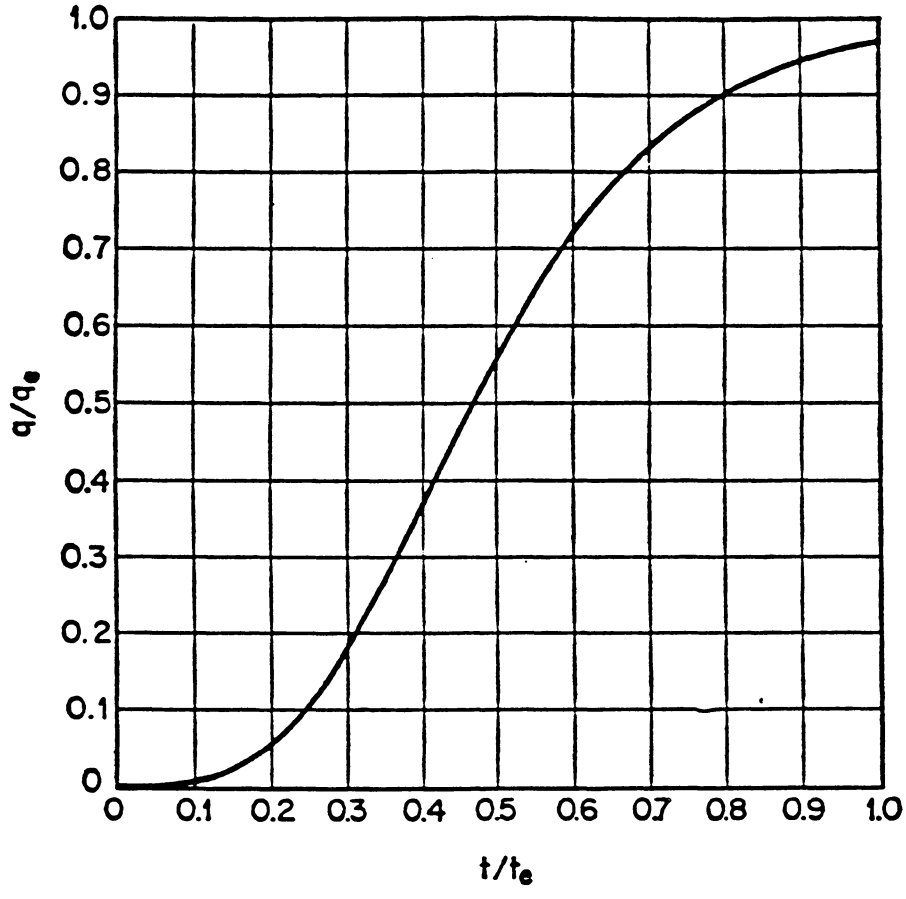

Figure 1. Izzard's dimensionless hydrograph for overland flow(from Chow, 1959, p. 542).

determined, per unit width of runoff plane, by multiplying the dimensionless q/q_e by QE(N). Discharge, in cubic feet per second, is determined by multiplying q by the width of the runoff plane. The runoff plane width was estimated as the circumference of half of the runoff length around the sinkhole subbasin.

Overland flow discharges were converted to potential energy for input to the sinkhole using the Bernoulli equation:

$$\Phi = \frac{(Q/A)^2}{2g} + \frac{p}{\gamma} + \text{ELEV} \qquad (4)$$

where: Φ = potential head, in feet of water,
Q = discharge of water, cubic feet per second,
A = cross-sectional area of depth of flow,
$(Q/A)^2/2g$ = velocity potential,
p/γ = depth of flow potential,
and, ELEV = elevation head or altitude difference between sinkhole and spring.

The elevation head was estimated as 20% of the altitude difference between the sinkhole node and the spring. Water entering the ground-water flow system in karst usually falls downward from the sinkhole input to some base level where horizontal flow towards the spring occurs. The results of overland flow modeling are potentials which vary with time, which can be plotted on a potentiograph for input to sinkhole nodes.

Conduits transmitting ground water are fractures having different widths, different shapes, differing degrees of sinuosity, pools, and

conduit constrictions. The composite spring hydrograph is representative of the rainfall on different area sub-basins and flow through combinations of these above and below ground characteristics.

The problem is how to represent all these characteristics in a conceptual model for karst aquifer response to rainfall. The soils and vegetative cover can be mapped and mathematical estimates made as to their effect on surface runoff towards the funnel centers. The below-ground water-transmitting fractures have various shapes, lengths, roughnesses, and sinuosities. These characteristics must be lumped together as a single parameter of the subsurface flow regime. That single parameter is the representative fracture conductivities of the karst basin.

Energy in a Karst Aquifer

Rainfall excess introduced into the conduit system through the funnel input is an energy addition to the aquifer. This energy can be expressed by the Bernoulli equation as the sum of the velocity head, pressure head, and elevation head (all in units of length). The velocity head is an expression of the kinetic energy of moving rainfall excess as it travels overland and sinks into the ground at the funnel center (or the sinkhole sub-basin). The pressure head is the energy of

the weight of the fluid flow depth. The elevation head is the difference in elevation between the conduit taking runoff from the sinkhole and the spring at the base of the system. This elevation head, which affects the gradient in the system, is the most difficult to define in karst aquifers because input from the sinkhole subbasin may travel vertically downward as vadose flow for considerable distances before flowing horizontally towards the spring. Therefore, the elevation head used should not be the altitude of the sinkhole minus the altitude of the spring. Rather, we make an arbitrary estimate of 20 percent or 30 percent of this value.

The pressure head additions to the aquifer are transmitted through interconnecting fractures towards the spring somewhat similar to heat travelling through a metal bar. The pulse arrives at the spring and creates increased flow due to heads just upstream from the spring being greater than heads at the spring. As more water is added to the aquifer from runoff, greater heads are built up in the underground flow system.

Equations of Flow

Hydraulic conductivities of karst aquifers are composed of two factors: one characterizing the geometrical properties of fractures or conduits and the other describing the behavior of the transported fluid. The

problem involved requires the consideration of two main forces for the laminar flow regime: gravity and fluid friction.

An accepted approach to solution of viscous flow problems is by application of the Navier-Stokes equations for laminar flow of a newtonian fluid. These can be written, per unit volume in a one dimensional x-direction, as

$$\frac{\rho}{n} = -\frac{dp}{dx} - \frac{\gamma dz}{dx} + \frac{\mu}{n}\frac{d^2u}{dx^2} \qquad (5)$$

where: ρ = fluid mass density,
z = vertical direction,
u = x-direction velocity,
n = porosity of medium,
p = fluid pressure,
μ = dynamic viscosity of water,
and, γ = fluid specific weight.

Dimensions of these terms are located in the Glossary of symbols. Similar expressions are obtained for **y and z** coordinates using equation (5) except for the gravity term in the z-direction.

For steady, incompressible fluids Equation (5) can be written as:

$$\nabla^2 q = \frac{\gamma n}{\mu} \nabla(\Phi + z) \qquad (6)$$

where: ∇ = vector operator,
q = fluid discharge per unit width,
and, Φ = fluid potential.

By application of Hubbert's potential to the Φ term above Equation (6) may be expressed in one dimension as:

$$\frac{d\phi}{dx} = \frac{\mu}{\nu n} \frac{d^2u}{dy^2} \qquad (7)$$

where: ϕ = fluid potential,
and, ν = kinematic viscosity of water.

For the problem of steady, uniform, one dimensional, laminar, incompressible flow through a passage bounded by plane, impermeable boundaries the fluid velocity can be solved by integrating Equation (7) twice with respect to the boundaries and velocity profile shown in Figure 2 which gives the average seepage velocity for flow through a fracture (n=1 for a fracture).

$$v_x = - \frac{gw^2}{12\nu} \frac{d\phi}{dx} \qquad [L/T] \qquad (8)$$

where: v_x = average x-direction velocity,
w = fracture width of fracture transmitting water,
and, g = gravitational constant.

The amount of water transported during a given time in a section of fissure having unit depth of flow can be determined by:

$$q = \int_{-w/2}^{w/2} v(y)dy = \frac{-gw^3}{12\nu} \frac{d\phi}{dx} \qquad [L^2/T] \qquad (9)$$

where: q = fluid discharge per unit depth of flow in fracture.

Using the analogy of Darcy's law, the hydraulic conductivity of a fracture is:

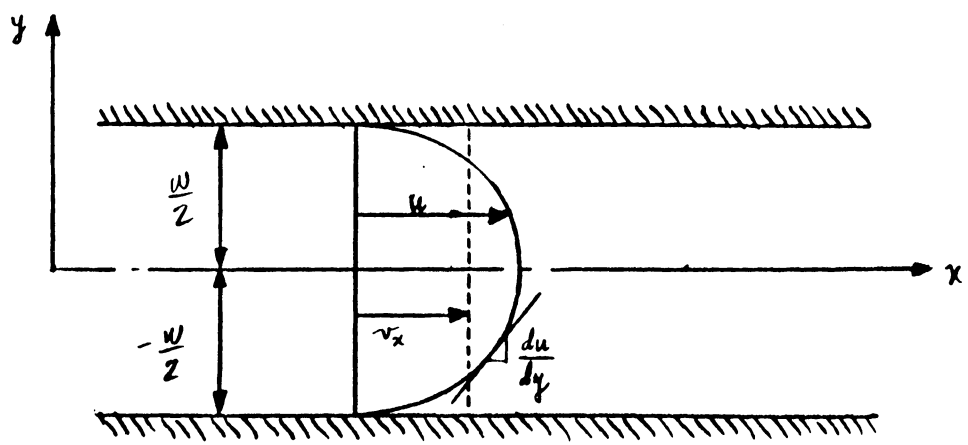

Figure 2. Boundaries and velocity profile for flow through a fracture

$$K = \frac{g\, w^{3}}{12\ \nu} \qquad (10)$$

It is necessary to note that there is a basic difference between the parameter determined by Equation (10) and Darcy's hydraulic conductivity. The latter, multiplied by the hydraulic gradient gives the seepage velocity, which is equal to the ratio of flow rate and total area normal to the flow direction and is thus smaller than the mean velocity in the pores. In contrast, Equation (8) immediately gives mean velocity and, therefore, the hydraulic conductivity of the fracture does not characterize the rock but only one opening.

The discharge Equation (9) is related to the potential gradient ($d\phi/dx$) in the system and the fracture conductivity. The representative fracture conductivities are dependent upon the gradient in the system in a fashion similar to depth of flow in a partially filled pipe carrying water. As heads increase in the system, cross-sectional area of flow increases, fracture conductivity increases, and discharge increases. A relationship can be established between potential gradient in a karst aquifer and different fracture conductivities. This relationship may be non-linear and can be determined by the finite element method due to the ability of the method to handle non-linear and time-dependent flow problems.

The nature of the application of the above principles and equations to flow of ground water in karst basins is based on the inability to

successfully apply analytical solutions to karst aquifers. Flow paths and varying conditions of flow regime can be dependent on many factors specific to each aquifer being investigated. The main restriction on the derivation of the equations of flow is that the flow must be laminar. This restriction is developed from experiments which modeled fluid flow through parallel plates (Huitt, 1956).

CHAPTER 3

FINITE ELEMENT FORMULATION OF GROUND-WATER FLOW

The flow of fluids through porous medium is governed by the general "quasi-harmonic" equation, the particular cases of which are the Laplace and Poisson's equations. Many categories of physical problems fall in the range of these governing equations. For the mathematical simulation of fluid flow in one dimension which includes time derivatives, the Poisson's equation is expressed as:

$$\frac{\partial}{\partial x}\left(K_x \frac{\partial \phi}{\partial x} \right) + \bar{Q} = \rho C \frac{\partial \phi}{\partial t} \qquad (11)$$

where: $\bar{Q}$ = source or sink term,
K_x = hydraulic conductivity in x-direction,
and, ρC = porosity or compressibility term.

If a situation at a particular instant of time is considered, time derivatives of the potential and other parameters can be treated as prescribed functions of space coordinates. These space coordinates are the essential principle of the finite element method whereby the local coordinate vector and the vector of unknowns are related to the global coordinate system as a one-to-one correspondence (Desai, 1977, p. 41-42).

Galerkin Formulation

While approximate minimization of a 'functional' is the most widely accepted means of arriving at a finite element numerical representation it is not the only means available. It is possible to arrive mathematically at the finite element approximation directly from differential equations governing the problem. One of these approaches is the Method of Weighted Residuals which is based on the minimization of the residual after an approximate or trial solution is substituted into the differential equations governing the problem. There are several methods available for selection of the weighting function. Galerkin's method is used in this study for the one-dimensional fluid flow problem applied to flow through fractures.

For the finite element formulation of ground-water flow using Galerkin's formulation, Equation (11) is arranged to represent one dimensional flow over domain Ω as:

$$\int_{\Omega} w_j \left\{ \left(K \frac{\partial^2 \phi}{\partial x^2} \right) + \left(\bar{Q} - \rho C \frac{\partial \phi}{\partial t} \right) \right\} d\Omega = 0 \qquad (12)$$

where: w_j = weighting function.

Equation (12) is subject to the natural boundary conditions for fluxes and geometric boundary conditions for specified sources. Integrating by parts, Equation (12) becomes:

$$\int_{\Omega}\{ - \frac{\partial v}{\partial x} \left(K \frac{\partial \phi}{\partial x} \right) + v \left(\bar{Q} - \rho C \frac{\partial \phi}{\partial t} \right) \} d\Omega$$

$$+ \int_{s} v \left(K \frac{\partial \phi}{\partial n} \right) + \int_{s} v \bar{q} \, dS = 0 \qquad (13)$$

where: $\bar{q}$ = flux term along surface s,
v = arbitrary functions,
s = surface of integration,
and, $\partial / \partial n$ = partial derivative normal to surface s.

For the Galerkin method, the integration variable v equals the one-dimensional, isoparametric element representation, $N=1/2(1\pm L)$(Desai, 1979). Substituting and arranging in matrix form, Equation (13) becomes:

$$[K] \{ \phi_n \} + [P] \{ \dot{\phi}_n \} = \{ f \} \qquad (14)$$

where: $[K] = \int [B]^T [R][B]$ = stiffness matrix,
$[B]$ = gradient-potential transformation matrix,
$[R]$ = vector of material properties,
$\{\phi_n\}$ = vector of unknown nodal potentials,
$[P] = \int \rho_c [N]^T [N] dV$ = damping matrix due to ρ_c,
$\{f\} = \int \bar{Q} [N]^T dV$ = load vector,
$\{\dot{\phi}_n\}$ = time derivative of $\{\phi_n\}$.

Initial and Boundary Conditions

Physical representation of specified initial conditions are the base-flows or low-flow of the karst aquifer. Specified source potentials ($\bar{Q}$ in Equation 13, in units of feet) are the known input to the system as a result of rainfall-runoff or as input to the fracture system from sinkhole nodes. Fluxes ($\bar{q}$ in Equation 13, in units of cubic feet per second) introduced at elements are the results of fluid input to the system due to the soil storage or porous storage. The specified source potentials are the kinetic, pressure, and elevation heads expressed by Bernoulli's equation.

At sinkhole nodes, the potentials specified by rainfall input to the sinkhole nodes are added to the initial conditions(or baseflow). These boundary conditions are held in the vector of unknowns $\{\phi_n\}$ for the solution procedure. The inputs from rainfall affect the model results the greatest.

The initial conditions are input as potentials at each node and represent the base flow of the system. The base flow potentials were set to 0.2 feet of head for the problem. Fluxes represent the soil or rock storage contribution to each element in the system. The magnitude of fluxes, when varied, appear to affect the results dramatically.

Therefore, fluxes are varied for the verification phase to determine the best match of the modeled discharges to the observed discharge data.

Estimates of porosity also dramatically affect solutions. Porosity may represent the characteristics of the fractures themselves or the characteristics of the entire basin. Porosity of a fracture will usually be equal to unity unless severe constrictions in the fractures prevent rapid fracture flow. The porosity of the basin is the volume of voids within the volume of rock in the aquifer. Solutions are presented based on different fluxes and different porosities in order to compare the results.

Solution Procedure

To solve the matrix form of the differential equations of flow, a finite difference approximation is made for the time derivatives in matrix notation:

$$\left\{ \frac{\partial \phi_n}{\partial t} \right\} = \frac{1}{\Delta t} \left(\{ \phi_n \}^{t+\Delta t} - \{ \phi_n \}^{t} \right) \qquad (15)$$

where t represents the time level and Δt is the length of each time step. $\{\partial \phi_n / \partial t\}$ is the column matrix whose individual entries are the

values of the potentials to be solved at each node n at the particular time. Equation (15) can be rearranged to have all the heads at the old time to be on the right-hand side and all the heads at the new time on the left-hand side. This is referred to as the forward finite difference solution. This technique is conditionally stable when time steps(Δt) are small so that ($\rho_c \Delta t / \Delta z^2$) $\leq 1/2$, where Δz=element length. The solution of the matrix of unknowns is obtained by the Gauss-Doolittle elimination procedure (Desai and Abel, 1972).

CHAPTER 4

KARST AQUIFER RESPONSE TO RAINFALL

There are two phases of model development. The calibration phase is where known data are input into the model and the parameters changed upon each iteration until the calculated values match the known observations. A relationship is established, which in this model is the relationship of potential gradient to fracture conductivity. In the verification phase, new data are input to the model and calculations performed based on the relationship established in the calibration phase. The output is compared to observed data for verification. Parameters may need to be additionally adjusted for the modeled values to match the observation data.

The one-dimensional finite-element model (called HYDMATCH) formulated in the previous sections is applied to an example karst basin to test the performance of the model. The mesh information, boundary conditions, sub-basin runoff hydrographs, the observed spring discharge hydrograph, and initial arbitrary fracture conductivities are input into HYDMATCH. The model calculates potentials at each node in the mesh for each time element specified. The flow chart for HYDMATCH is shown in Figure 3.

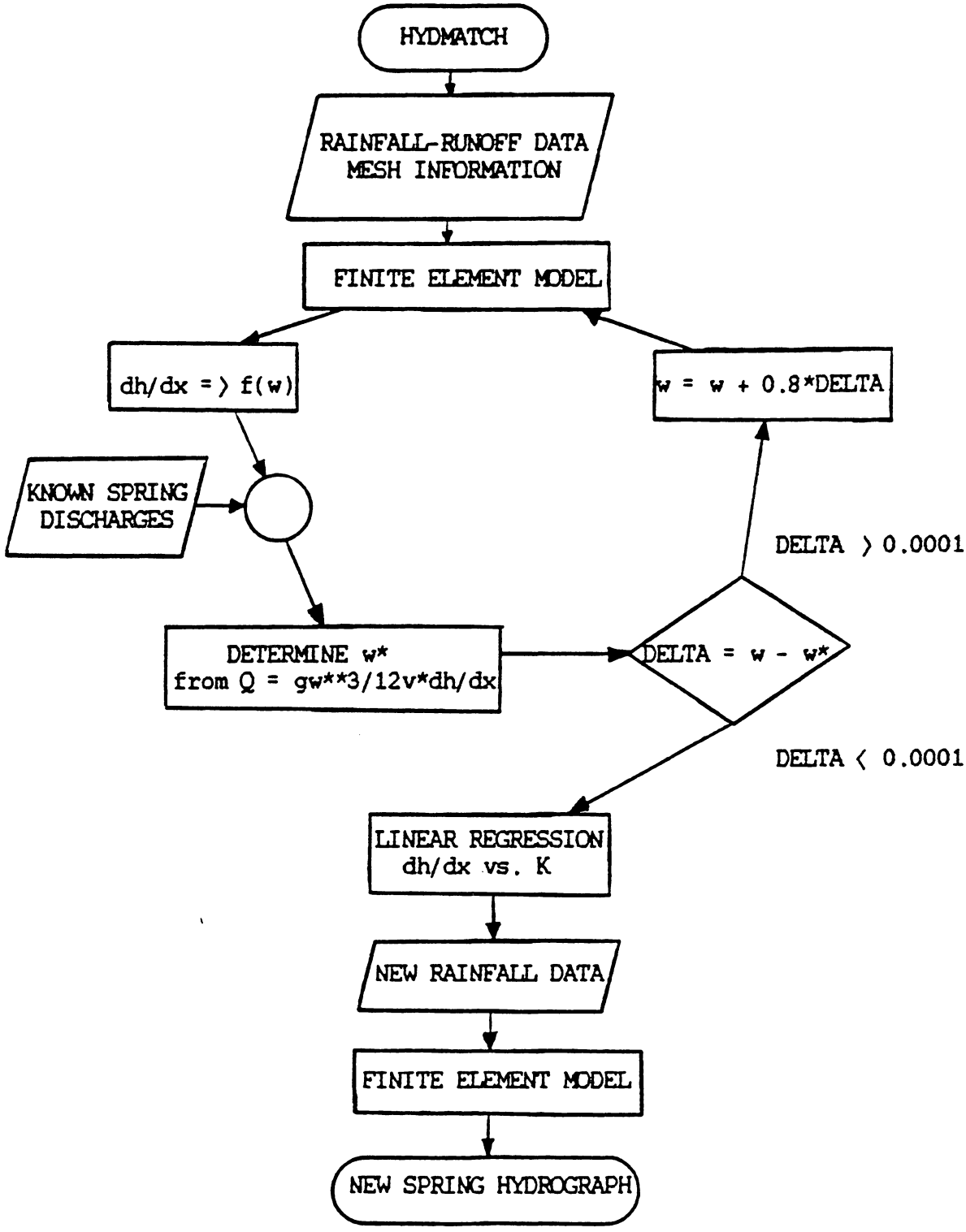

Figure 3. Flow chart for HYDMATCH.

For the first iteration, the solution for potentials at each node in the mesh is solved with each element having the same fracture conductivity--an initial arbitrary fracture conductivity. At the end of each successive iteration, a relationship between fracture conductivity and potential gradient is established as follows. The observed discharges from the spring hydrograph are used to determine what the fracture conductivities should be corresponding to the potential gradient. Recall equation (9):

$$q = \frac{g w^3}{12 \nu} \frac{d\phi}{dx} \tag{9}$$

The discharges are known from the spring hydrograph and potential gradients are known from the finite-element solution. Solving for fracture conductivity:

$$K = q \cdot dx/d\phi$$

In order to normalize the fracture conductivities for iterative comparison, the fracture widths from the current iteration are compared to the fracture widths of the last iteration. The fracture width is calculated from equation (9):

$$w = (q \cdot 12\nu \cdot dx/g \cdot dh)^{1/3} \tag{16}$$

Iterations are repeated until the difference is small between the current fracture widths and the previous iteration fracture widths. When this convergence has been completed, a linear regression equation is established (Ang and Tang, 1975) between fracture conductivity and potential gradient.

Example Karst Basin

The city of Roanoke, Virginia is built on a karst aquifer developed in the Elbrook dolomite (Figure 4). A study was performed in Roanoke by the U.S. Geological Survey to determine the response of springs in the area to rainfall (U.S. Geological Survey, unpublished data, 1982). Data for spring hydrographs indicate that secondary permeabilities are a significant factor contributing to rapid ground-water velocities and recharge to the aquifer from rainfall.

Discretization of the finite element mesh considers sinkholes in subbasins I, II, III, and IV as the input nodes to Nininger spring (Figure 5). The element placements assume that the sinkholes are related to subsurface conduits. Other sinkholes in the subbasins are considered as part of the runoff plane.

The computer program for rainfall-runoff modeling, described in the previous section, was used to determine overland flow input to sinkhole nodes. The subbasin characteristics used in the model are shown in

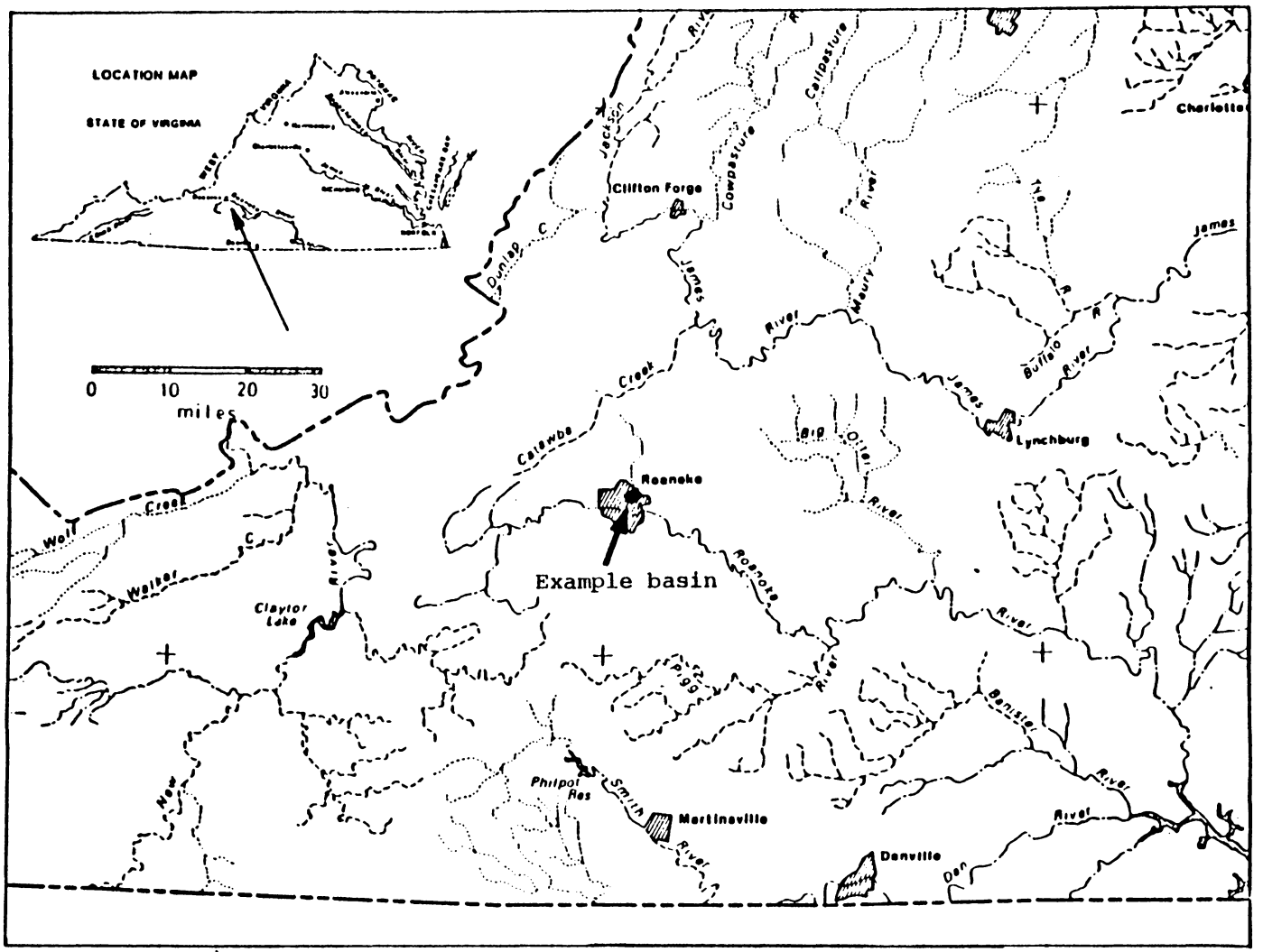

Figure 4. Location map of example karst basin

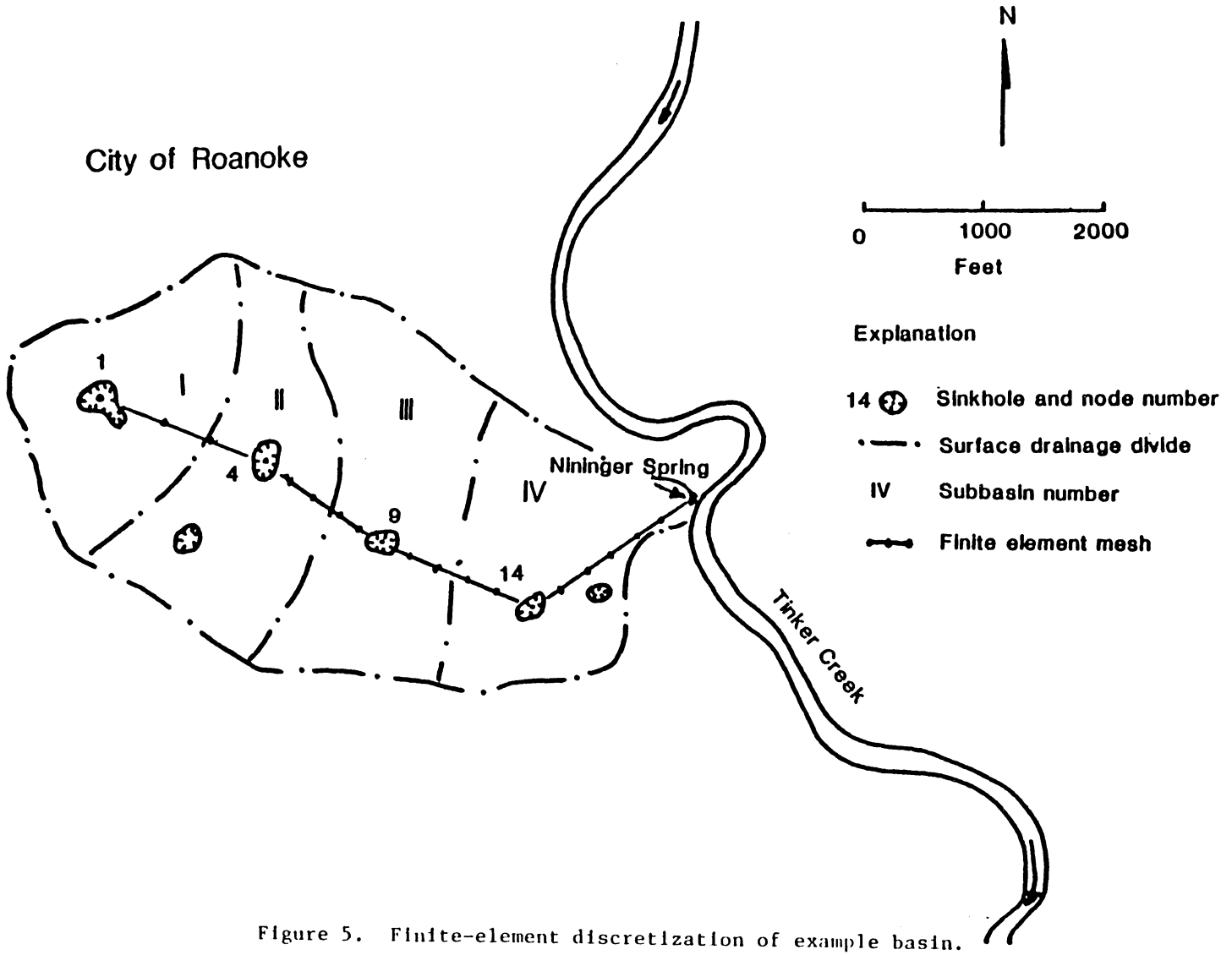

Figure 5. Finite-element discretization of example basin.

Table 1. The rainfall-runoff model generated potentiographs for a one-half inch rainfall (shown in Figure 6). These were used for input to the ground-water model for the calibration phase. Rainfall data were modeled and potentiographs produced for a one-inch rainfall (not shown graphically) for the verification phase of the ground-water model.

Table 1. Subbasin characteristics for input to HYDMATCH.

Subbasin characteristics for input to node 1.

Length of runoff plane	= 846 feet
Slope of runoff plane	= 0.035 ft/ft
Roughness of runoff plane	= 0.035
Width of runoff plane	= 923 feet
Elevation head of node	= 20 feet

Subbasin characteristics for input to node 7.

Length of runoff plane	= 1230 feet
Slope of runoff plane	= 0.016 ft/ft
Roughness of runoff plane	= 0.035
Width of runoff plane	= 923 feet
Elevation head of node	= 12 feet

Subbasin characteristics for input to node 12.

Length of runoff plane	= 1540 feet
Slope of runoff plane	= 0.020 ft/ft
Roughness of runoff plane	= 0.035
Width of runoff plane	= 1000 feet
Elevation head of node	= 6 feet

Subbasin characteristics for input to node 17.

Length of runoff plane	= 1500 feet
Slope of runoff plane	= 0.040 ft/ft
Roughness of runoff plane	= 0.035
Width of runoff plane	= 900 feet
Elevation head of node	= 3 feet

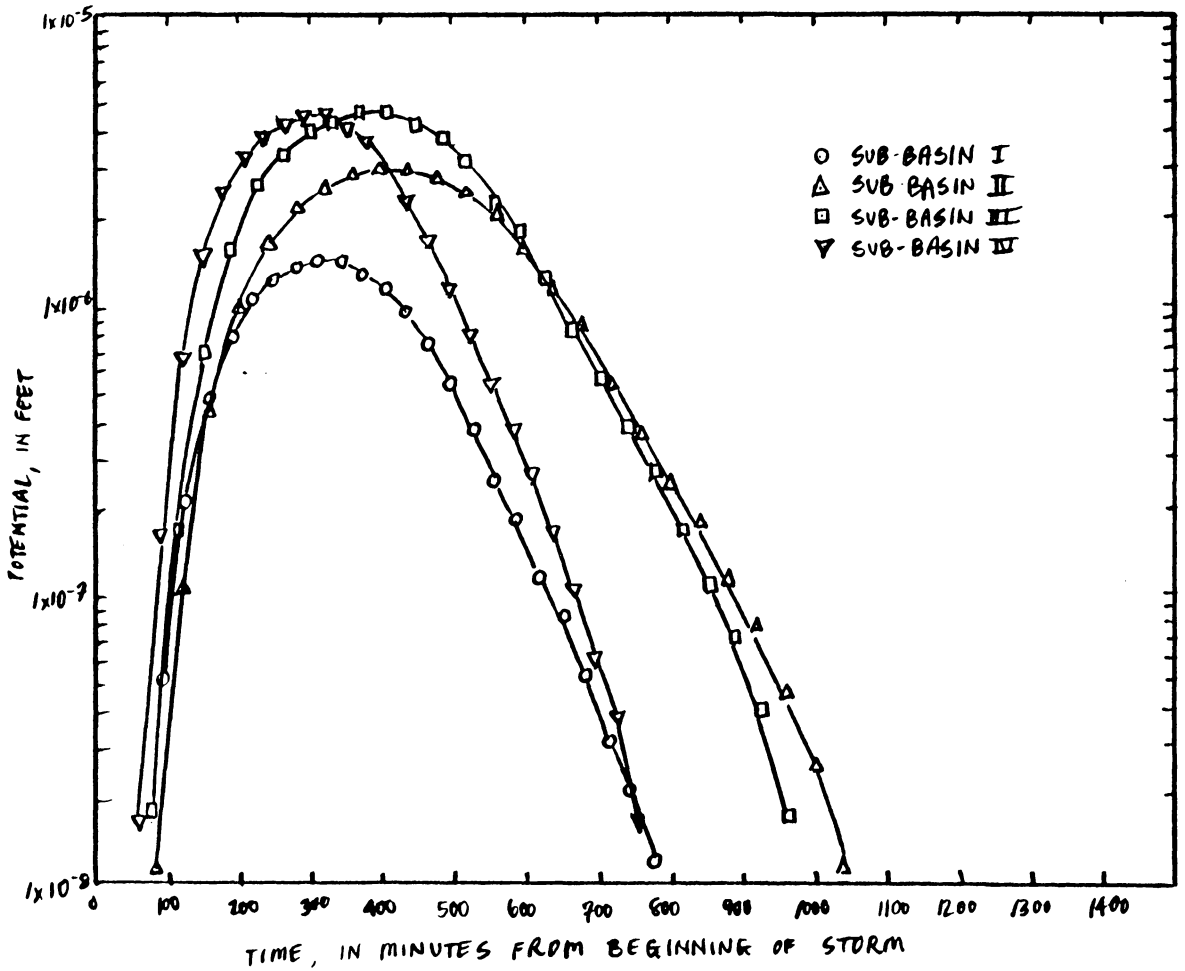

Figure 6. Overland runoff potentiograph from sub-basins for one-half inch rainfall

Results

The results of potential gradient versus fracture conductivity based on a one-half inch rainfall for different scenarios and the modeled spring hydrographs in response to a one-inch rainfall are shown in Figures 7 through 18. The modeled hydrographs are compared to an actual hydrograph from Nininger spring in response to a one-inch rainfall. Results are shown where the porosity and flux parameters were varied.

The modeled discharges from the one-inch rainfall for porosity equal to 1.0 and fluxes equal to 0.0001 (in units of cubic feet per second) compare well with the actual discharges as shown in Figure 8. The hydrograph peaks are at similar times and the discharge magnitudes are almost the same. The main difference is the shape of the recession curves. The differences are probably due to soil storage and discrepancies in actual rainfall-runoff and calculated rainfall-runoff. The jump in the potential versus fracture conductivity graphs (between the third and fourth data points) may be due to matching the rising limb of the given hydrograph.

The results indicate that setting the porosity equal to unity is most representative of spring response to the rainfall input. The value of one of flux (in cubic feet per second) is not like one of porosity--however, fluxes on the order of 10^{-4}, combined with the rainfall input

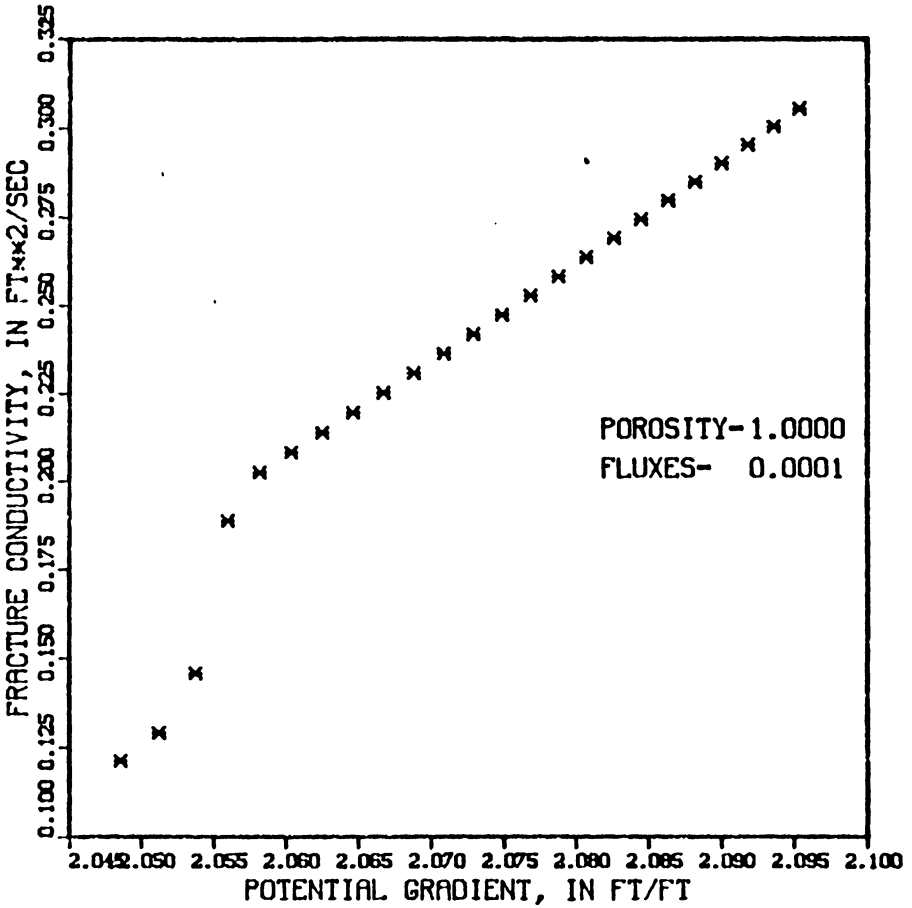

Figure 7. Potential gradient versus fracture conductivity determined from spring hydrograph data for one-half inch rainfall(flux units are in cubic feet per second).

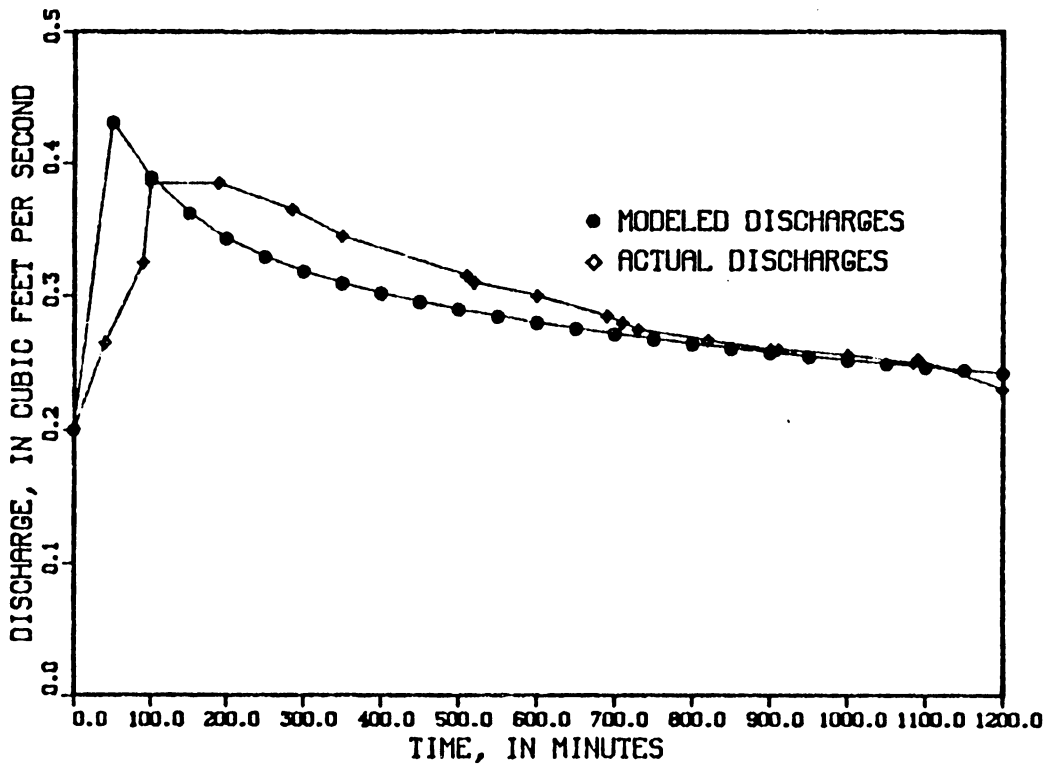

Figure 8. Modeled discharges compared to actual discharges for one-inch rainfall. Modeled discharges determined using potential gradient versus fracture conductivity relationship in figure 8.

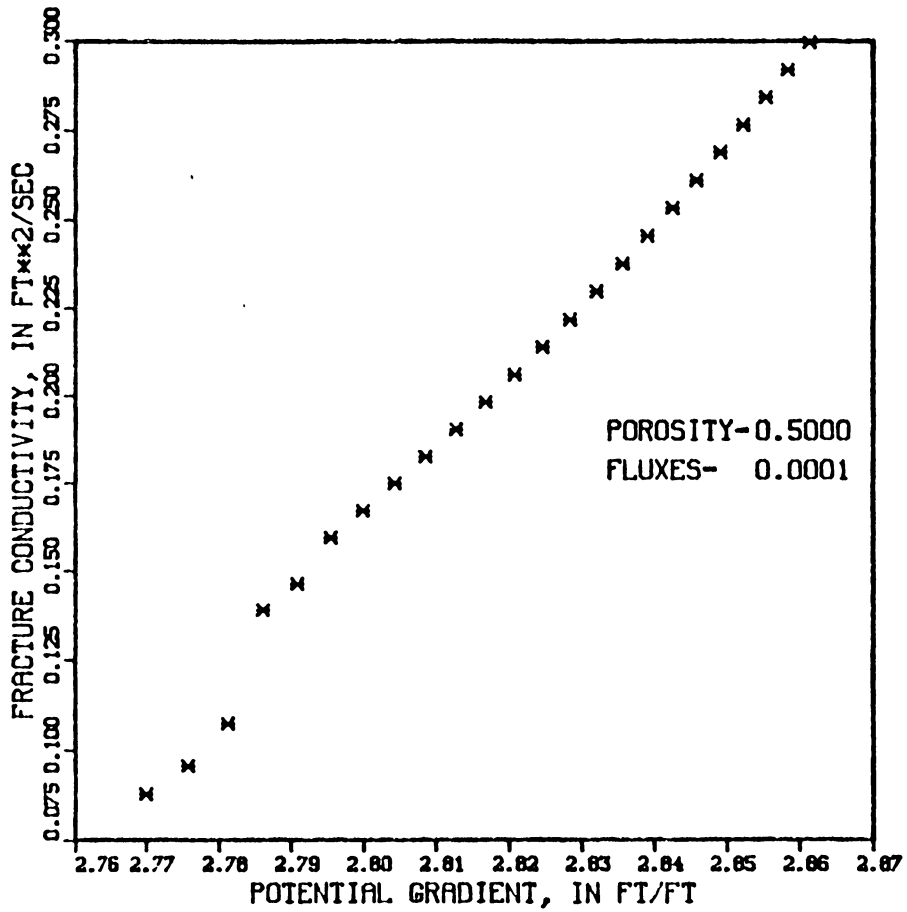

Figure 9. Potential gradient versus fracture conductivity determined from spring hydrograph data for one-half inch rainfall(flux units are in cubic feet per second).

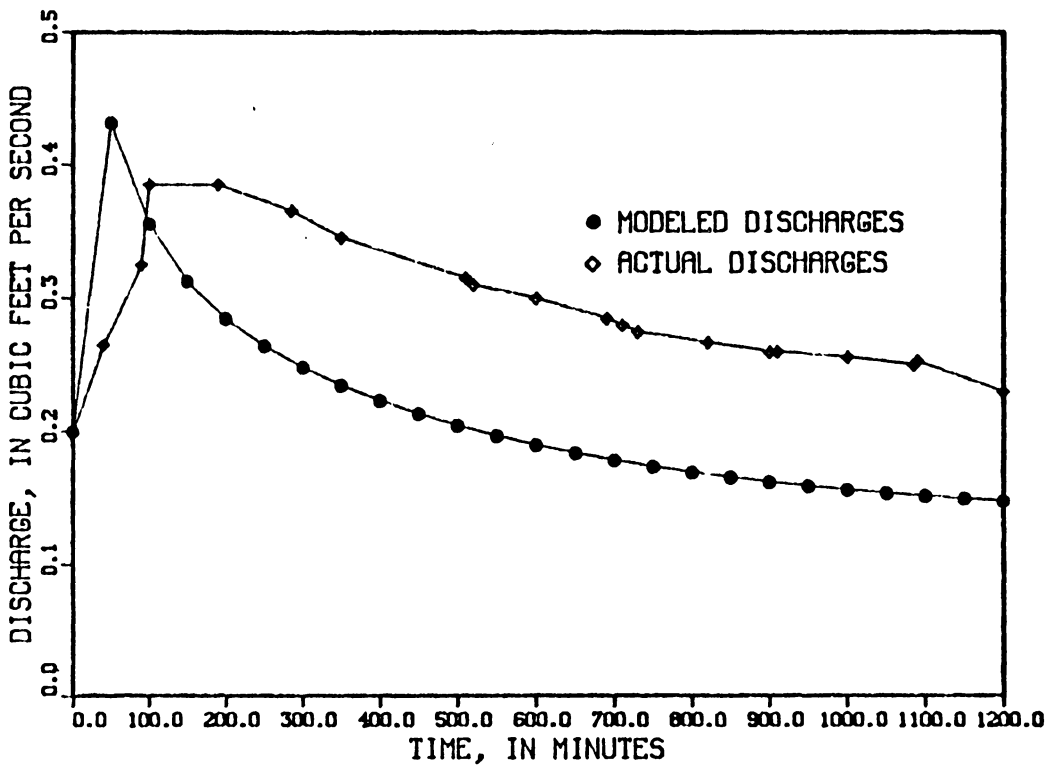

Figure 10. Modeled discharges compared to actual discharges for one-inch rainfall. Modeled discharges determined using potential gradient versus fracture conductivity relationship in figure 10.

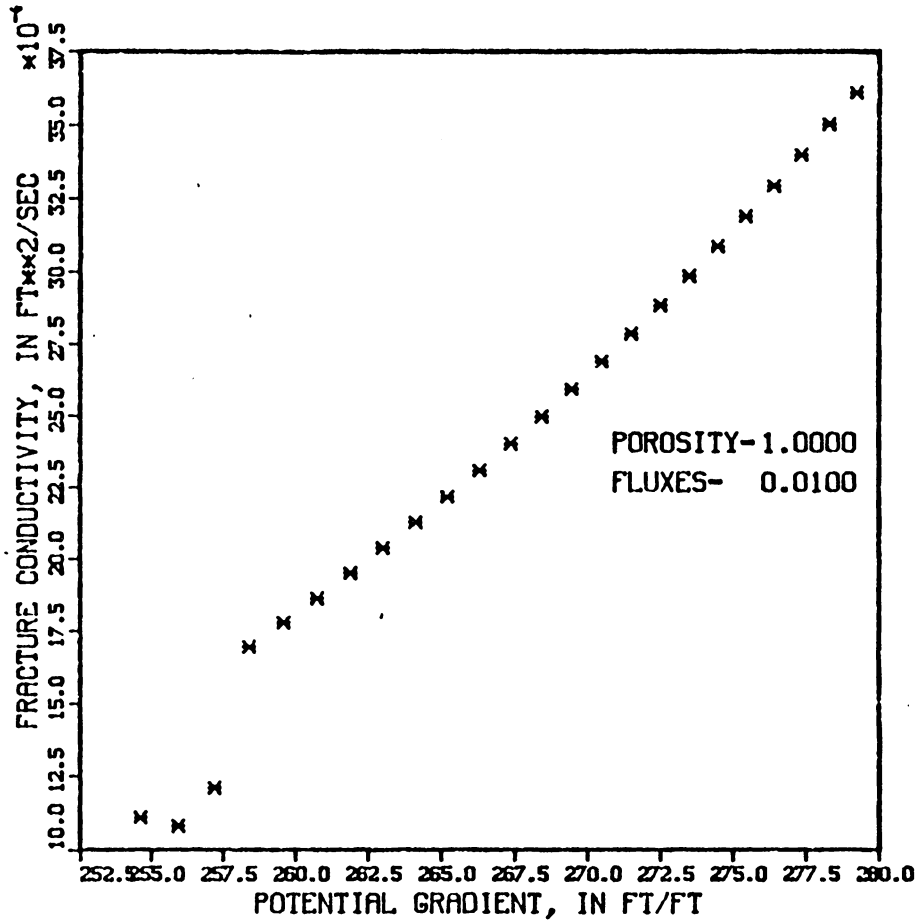

Figure 11. Potential gradient versus fracture conductivity determined from spring hydrograph data for one-half inch rainfall(flux units are in cubic feet per second).

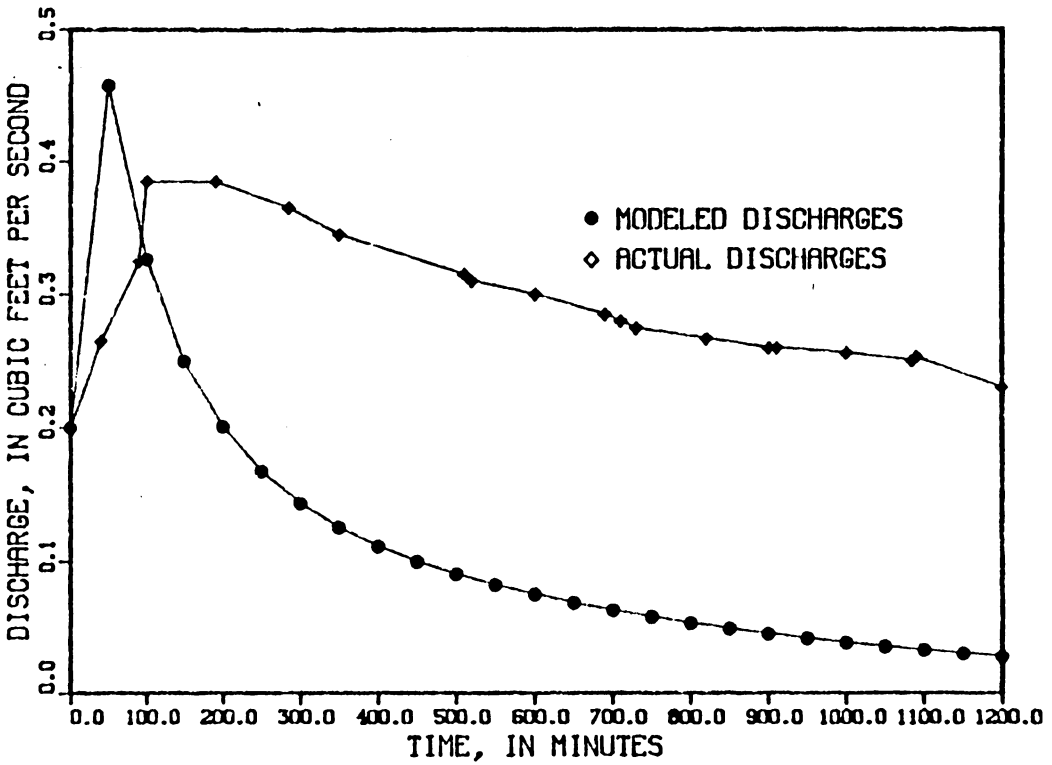

Figure 12. Modeled discharges compared to actual discharges for one-inch rainfall. Modeled discharges determined using potential gradient versus fracture conductivity relationship in figure 12.

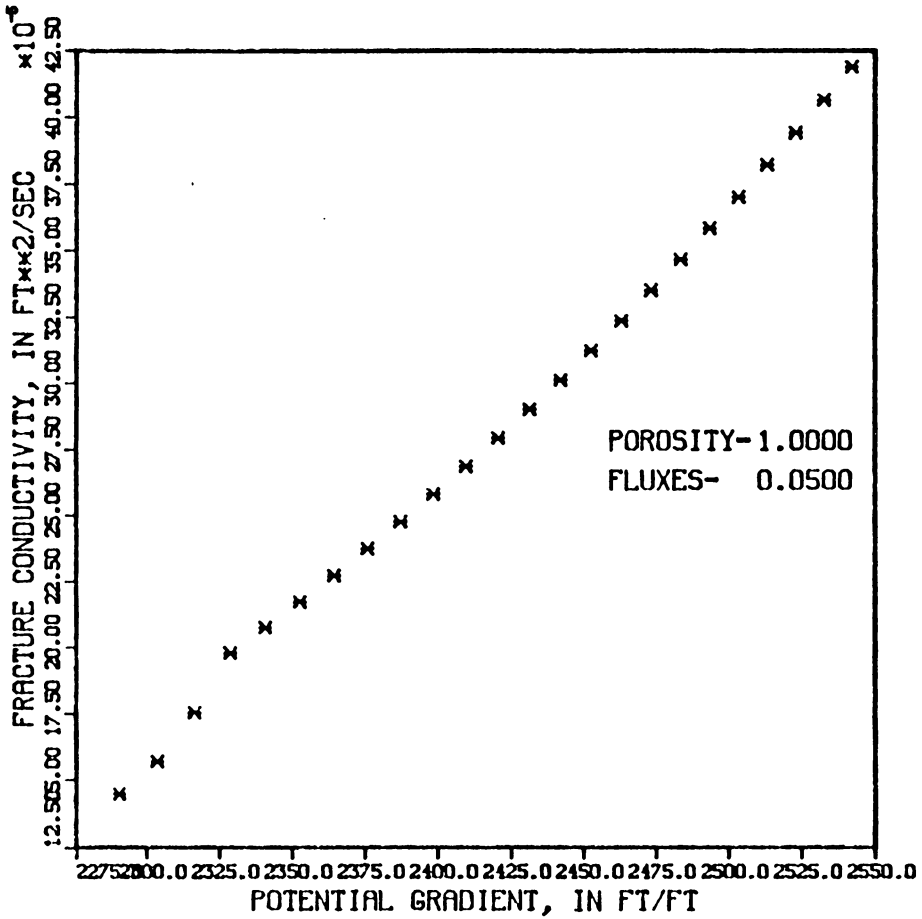

Figure 13. Potential gradient versus fracture conductivity determined from spring hydrograph data for one-half inch rainfall(flux units are in cubic feet per second).

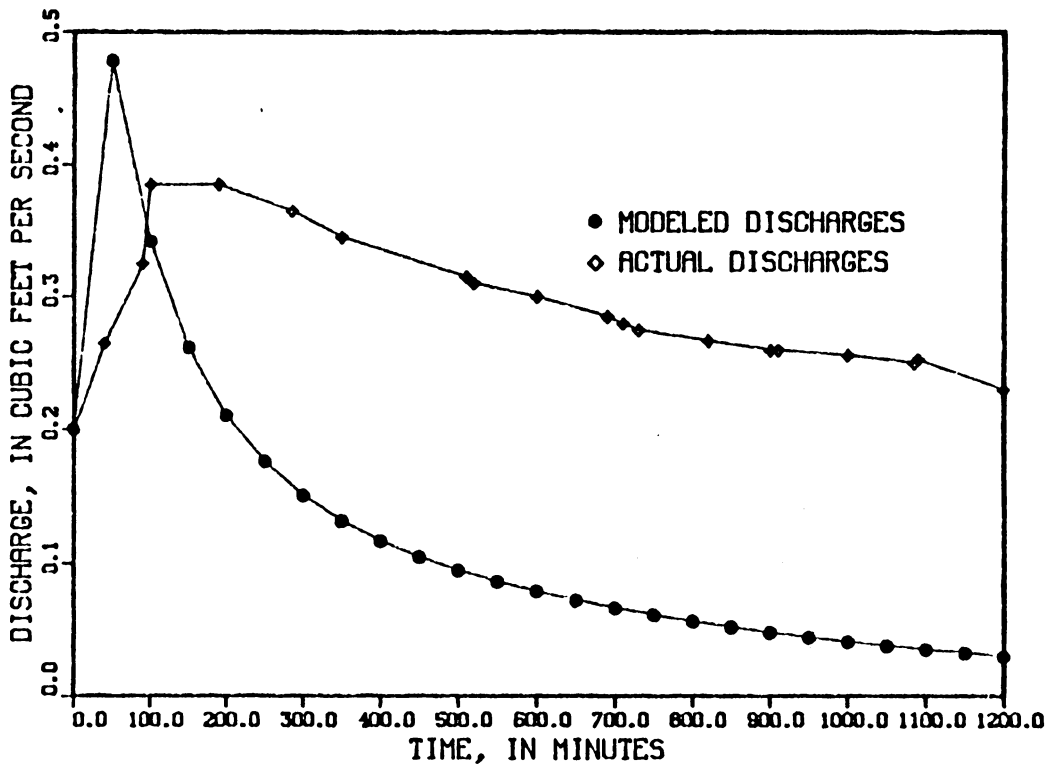

Figure 14. Modeled discharges compared to actual discharges for one-inch rainfall. Modeled discharges determined using potential gradient versus fracture conductivity relationship in figure 14.

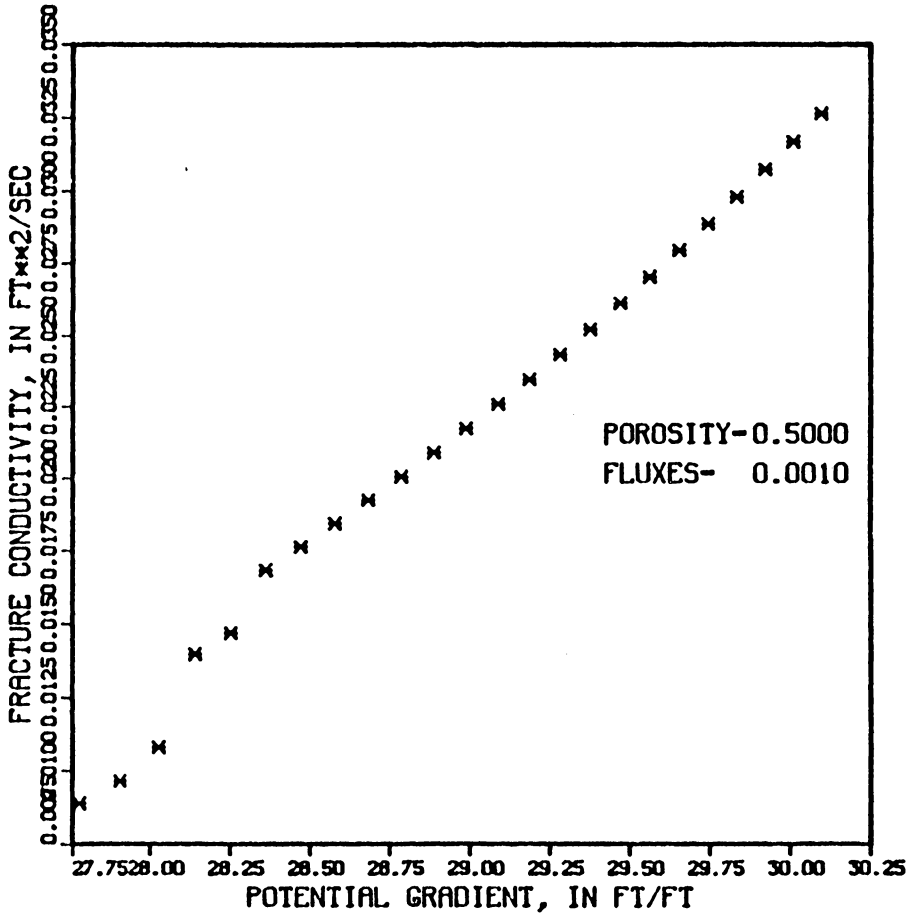

Figure 15. Potential gradient versus fracture conductivity determined from spring hydrograph data for one-half inch rainfall(flux units are in cubic feet per second).

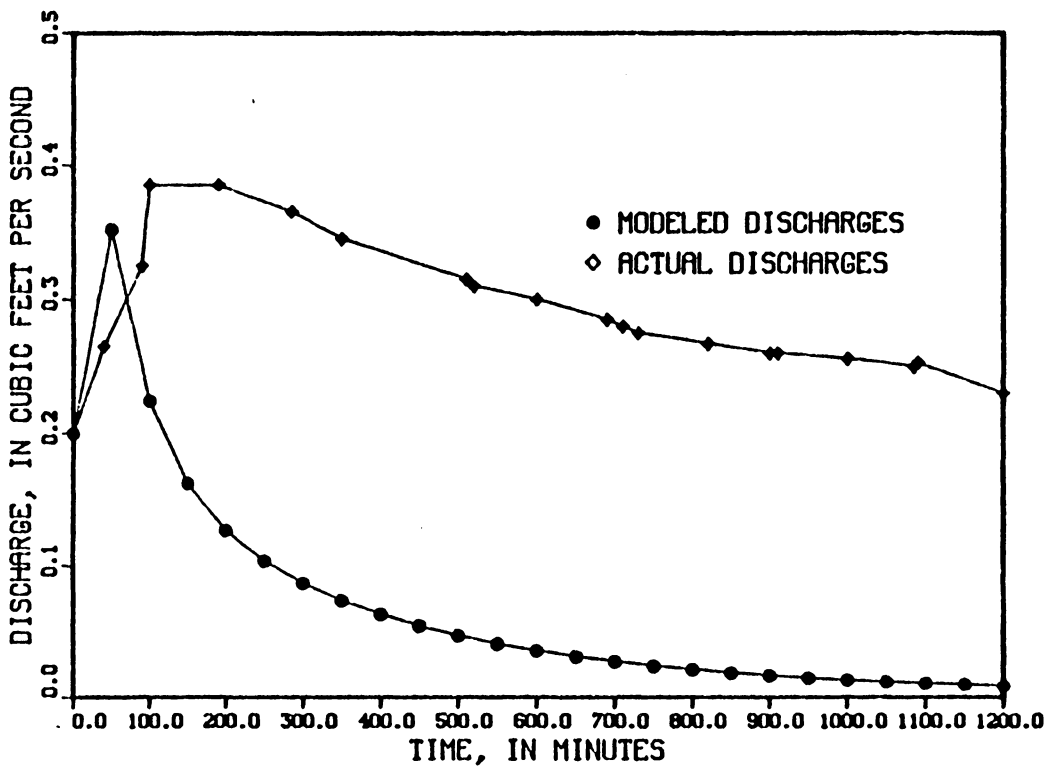

Figure 16. Modeled discharges compared to actual discharges for one-inch rainfall. Modeled discharges determined using potential gradient versus fracture conductivity relationship in figure 16.

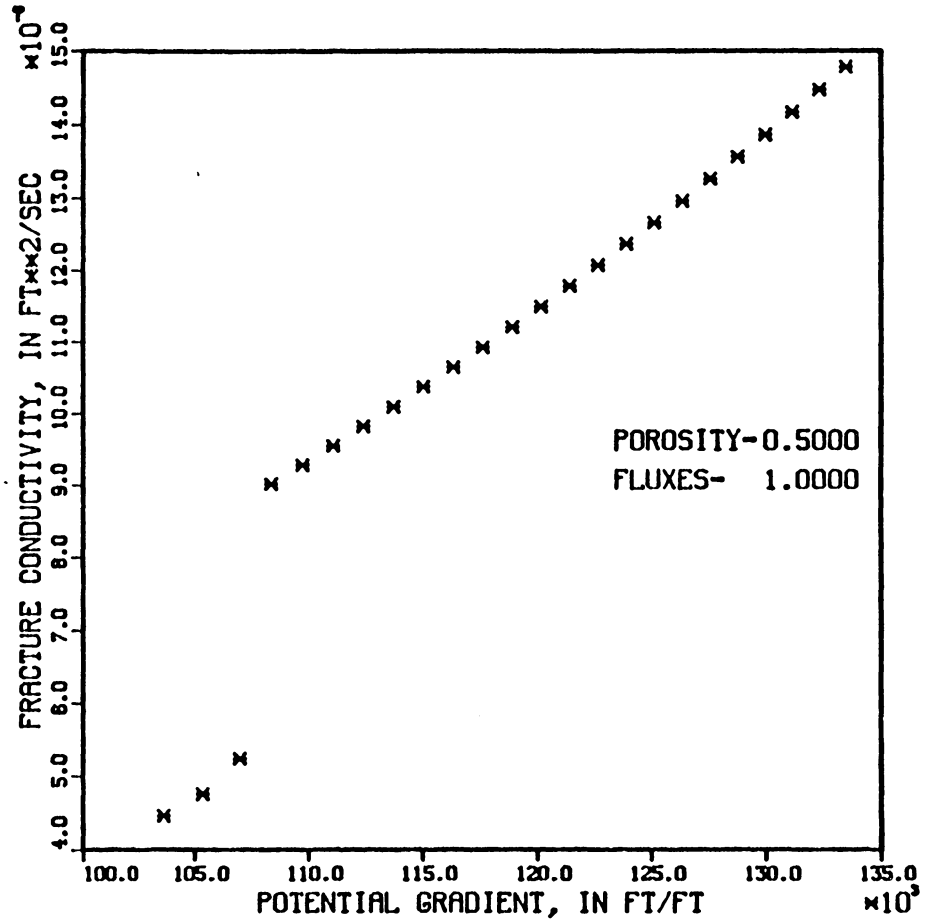

Figure 17. Potential gradient versus fracture conductivity determined from spring hydrograph data for one-half inch rainfall(flux units are in cubic feet per second).

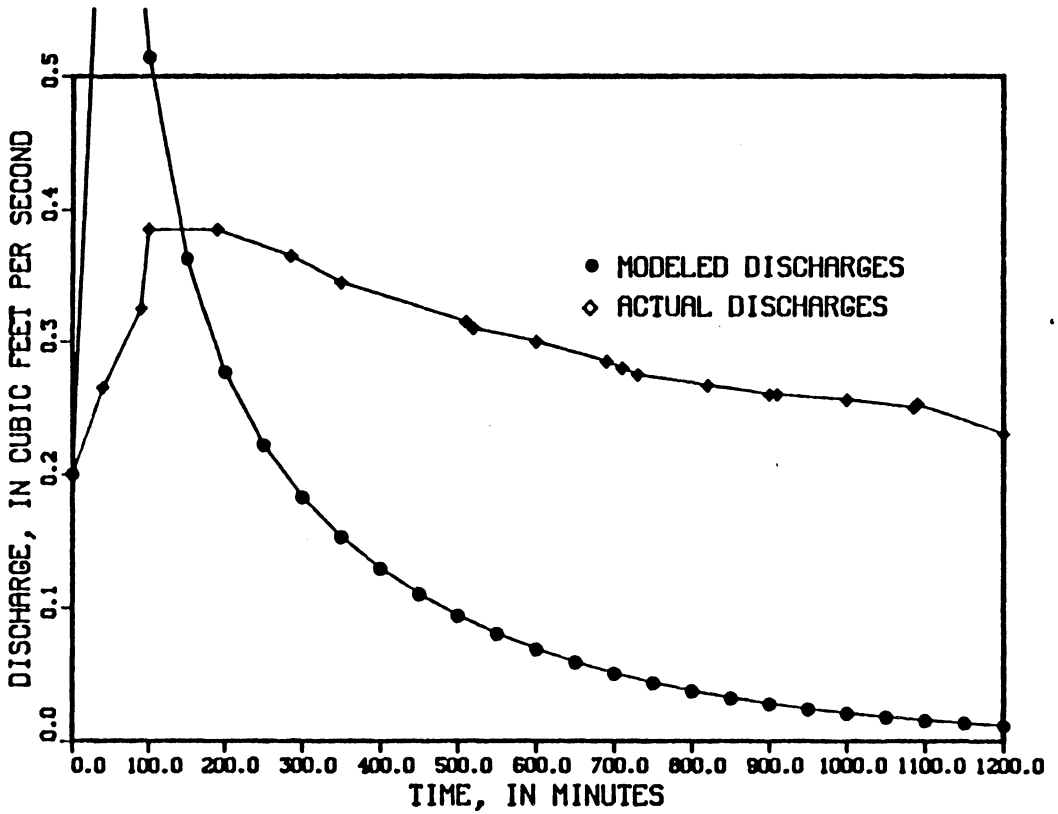

Figure 18. Modeled discharges compared to actual discharges for one-inch rainfall. Modeled discharges determined using potential gradient versus fracture conductivity relationship in figure 18.

and initial conditions, produce reasonable results. This represents an accurate statement of a typical karst aquifer system: discrete fractures (porosity = 1) providing rapid transport of ground-water recharge and small but significant soil storage or fracture storage in the karst aquifer.

One problem with the results is that the Reynolds numbers were too high. This non-dimensional number is a determination of the flow regime of flowing water-- whether laminar or turbulent. If the flow exceeds the laminar range, then approximations made deriving the equations presented in the previous sections are no longer valid. The Reynolds numbers for the simulation of ground-water flow in the example karst basin exceeded 10^5. Fluid flow in simulated fractures is expected to be in the turbulent range when Reynolds numbers exceed 4,000 (Huitt, 1956).

CHAPTER 5

SUMMARY AND CONCLUSIONS

The finite-element model (called HYDMATCH) is successful at taking known spring discharge data from a karst aquifer and generating a linear regression relationship for potential gradient versus fracture conductivity in the system. This relationship is then used to generate hydrographs for other rainfall events on the karst basin. There are many difficulties to be faced trying to model ground-water flow in a karst aquifer -- not only in the conceptualization but also in parameter estimation and model execution. The success shown here is an indication that with more work in the problem areas, rainfall-runoff in karst areas can be modeled using the finite element method.

The problem areas with modeling karst ground-water flow are: 1) conceptualization of hydrogeologic framework in karst areas, 2) rainfall-runoff in circular shaped basins for input to sinkhole nodes, 3) estimation of base flows and flux contributions to the karst aquifer, 4) determining catchment areas which contribute to karst aquifers, and 5) estimating the elevation head for energy calculations in karst aquifers.

Areas in need of additional work with the finite-element model are: 1) the depth of flow in the fractures was set equal to one in order to

multiply the fracture discharge per unit depth (q) by depth to obtain discharge in cubic feet per second, 2) the model can deal with simple one-dimensional mesh only, i.e. the finite element mesh is established by sinkholes that are in line(indicating interconnected subsurface conduits). Therfore, sinkholes within the catchment which are not alined with the main conduits will not be included in the finite-element mesh, and 3) Reynolds numbers for fracture flow in the karst aquifer are too high.

Application of HYDMATCH to other karst aquifers would better test the performance of the model. Using the model on a larger karst basin may produce results that are closer percentage-wise to the actual event. In such a large basin application, errors in catchment area estimation may not affect the results so severely.

REFERENCES

Ang, A., and Tang, W. H., Probability concepts in engineering planning and design: John Wiley and Sons, Inc., New York, 409 pp.

Chow, Ven Te, 1959, Open-channel hydraulics: McGraw-Hill, New York, 680 pp.

Desai, C. S., 1979, Elementary finite element method: Prentice-Hall, Inc., New Jersey, 434 pp.

Desai, C. S., and Abel, J. F., 1972, Introduction to the finite element method: Van Nostrand Reinhold Company, New York, 477 pp.

Eagleson, Peter S., 1970, Dynamic hydrology: McGraw-Hill, New York, 462 pp.

Holtan, H. N., and Lopez, N. C., 1971, Model of watershed hydrology: U.S. Department of Agriculture, Technical Bulletin number 1435.

Huitt, J. L., 1956, Fluid flow in simulated fractures: American Inst. of Chemical Engineering Journal, v. 2, n. 2, p. 259-264.

LeGrand, H. E., 1973, Hydrological and ecological problems of karst regions: Science, v. 179, p. 859-864.

Pinder, G. F., and Gray, W. G., 1977, Finite element simulation in surface and subsurface hydrology: Academic Press, New York, 295 pp.

Stringfield, V. T., and LeGrand, H. E., 1969, Hydrology of carbonate rock terranes--a review: Journal of Hydrology, v. 8, p. 349-376.

Thrailkill, John, 1974, Pipe flow models of a Kentucky limestone aquifer: Ground Water, v. 12, n. 4, p. 202-205.

Torbarov, K., 1976, Estimation of permeability and effective porosity in karst on the basis of recession curve analysis: in Karst Hydrology and Water Resources, Volume 1, Water Resources Publications, Fort Collins, Colorado, p. 121-136.

White, William B., 1969, Conceptual models for carbonate aquifers: Ground Water, v. 7, n. 3.

GLOSSARY OF SYMBOLS

Symbol	Definition and dimensions
g	Gravitional constant (Lt^{-2})
h	Potentiometric head (L)
n	Porosity (dimensionless)
p	Fluid pressure intensity (FL^{-2})
q	Discharge per unit width (L^2t^{-1})
t	Time (t)
u	Component of x-direction fluid velocity (Lt^{-1})
v	Velocity (Lt^{-1}); subscript indicates direction
w	Fracture width (L)
x	Coordinate direction (L); horizontal coordinate
y	Fluid flow depth coordinate (L)
z	Coordinate direction (L); vertical coordinate
C	Constant (dimensionless)
$[K]$	Element property matrix
K	Permeability or hydraulic conductivity (Lt^{-1})
L	Local coordinate length (dimensionless)
N	Interpolation function
Q	Vector of specified source potentials
W	Minimization function
γ	Fluid specific weight (FL^{-3})
μ	Dynamic viscosity ($FL^{-2}t$)
ν	Kinematic viscosity (L^2t^{-1})
Φ, ϕ	Potential head (L)
ρ	Fluid mass density ($FL^{-4}t^2$)
∇	Vector operator
Ω	Domain of integration
$\{\phi_n\}$	Time derivative of potential vector with n nodes in finite element mesh
∂	Partial differential
d	Total differential
s	Surface of integration
v	Arbitrary function
w_j	Weighting function

The vita has been removed from the scanned document